Tellus (1979), *31*, 351–371

Observations of stratified flow over two-dimensional obstacles in fluid of finite depth

By P. G. BAINES, *CSIRO Division of Atmospheric Physics, P.O. Box 77, Mordialloc, Victoria 3195, Australia*

(Manuscript received October 24, 1978; in final form April 5, 1979)

ABSTRACT

This paper describes the results of an experimental study of stratified flow over two-dimensional obstacles in fluid of finite depth, with large Reynolds numbers and obstacle heights of about $\frac{1}{16}$ channel depth or less. Both long and short obstacles have been used, and all aspects of the flow field are described in some detail. The observations are compared with relevant theoretical results, notably those from the linearized small obstacle height model. For supercritical flows ($0 < K = ND/\pi U < 1$) the linear theory gives a quite accurate description of the flow right up to very close to the critical speed ($K = 1$), even though the linear model solution diverges as the critical flow speed is approached. For subcritical flows (where observations have been concentrated in the range where only the first lee wave mode is present ($1 < K < 2$)) the various properties of the lee wave field are reasonably well described by linear theory, but other aspects of the flow are not well described, particularly if the flow is just subcritical. Regardless of the smallness of the obstacle height, there is a finite parameter range ($1 < K < K_c$) where steady, columnar mode 1 structure is found upstream ("upstream influence"), in the same sense as described by Baines (1977) for larger obstacles, and this motion is not consistent with the small amplitude perturbation theory. This flow is apparently a permanent feature, with K_c tending to unity as the obstacle height h approaches zero. Flow fields over the obstacle show corresponding differences from linear theory, and similar behaviour occurs for the higher order modes. These phenomena must have a non-linear origin, and it is shown that they may be important in atmospheric flows.

1. Introduction

This paper describes an experimental study of stratified flow over two-dimensional obstacles in fluid of finite depth with large Reynolds number. We expect viscous effects to be of minor importance so that the flow may be adequately described by inviscid equations, and the results to be representative of geophysical flows, such as air flow over mountain ranges and oceanic flows over submarine ridges, when rotation is not important.

There have been many theoretical studies of inviscid stratified flow over obstacles, but relatively few corresponding experimental studies. Generally speaking, the theoretical studies may be classified into three groups: (i) linear models based on small perturbations of the horizontal flow, (ii) Long's steady-state, finite amplitude model and Yih's (1960) generalizations, and (iii) numerical studies. Of these the first is versatile, the simplest and the most commonly used. Long's model has been discussed in some detail in Baines (1977) and will not be considered extensively here. Numerical studies play an important role complementing that of the analytic studies, and the most significant recent contributions are those of Klemp and Lilly (1978) and Clark and Peltier (1977). However, so far there have been no numerical studies which cover the circumstances of the experiments being reported here, and we will concentrate on the linear models in this paper.

Linear models based on the assumption of small obstacle height were pioneered by Lyra (1943) and Queney (1948), and generalized by a number of other workers. Reviews of the subject from the meteorological standpoint may be found in Queney et al. (1960), Nichols (1973) and Gossard and Hooke (1975). The most complete mathematical formulation is by McIntyre (1972), who develops the solution as an expansion in powers of the

 0040-2826/79/040351-21$02.50/0

obstacle height. To date, the predictions of this model have not been compared quantitatively with experiments with continuous stratification, although previous experimental studies have made qualitative (Long, 1955; Davis, 1969) and quantitative (Baines, 1977) comparisons with the more ambitious Long's model. These studies show that substantial qualitative departure from the linear theory occurs if the obstacle height is large, in fluid of finite depth. Smith (1976) has made a quantitative comparison between linear theory and experiment for a two-layer configuration. For his particular parameter values (obstacle height $\sim\frac{1}{9}$ depth of lower layer) he found, in both the atmosphere and the laboratory, that the theory predicted the lee wavelength correctly but underestimated the amplitude by as much as a factor of four. He concluded that non-linear effects must be responsible for this discrepancy.

The aims of the current experiments are to provide a detailed description of stratified flow over two-dimensional obstacles when the obstacle height is (reasonably) small, and to compare the results with the predictions of linearized theory. The method and notation of McIntyre are used for this purpose.

In order to set up the theoretical framework for comparison with experiments, we consider a two-dimensional incompressible Bousinesq stratified fluid with constant Brunt-Väisälä frequency N, bounded above and below by two rigid horizontal boundaries separated by a constant depth D. An obstacle of height h is situated on the lower boundary, and this suddenly commences horizontal motion at speed U at time $t = 0$. We take x and z to be horizontal and vertical Cartesian coordinates, respectively, with axes fixed relative to the topography. u and w denote the corresponding fluid velocity components, and the perturbation stream function ψ is given by

$$u = U + \psi_z, \qquad w = -\psi_x, \tag{1.1}$$

where the suffices denote derivatives. We take the topography to have the form $z = hf(\pi x/D)$, where $0 \leqslant f \leqslant 1$. From the above quantities we may define three important dimensionless parameters:

$$K = \frac{ND}{\pi U}, \qquad R = \frac{Nh}{U}, \qquad \varepsilon = \frac{\pi h}{D} = \frac{R}{K}. \tag{1.2}$$

K is defined such that, if $n < K < n + 1$ for any integer $n > 0$, the first n stationary lee wave modes may exist (the notation employed here differs from McIntyre's in that here D denotes the total depth, whereas in his it denotes depth/π; the definition of K is the same). If $K < 1$ no linear waves may propagate upstream, so that the flow is supercritical; if $K > 1$ it is possible that the first wave mode (at least) may propagate upstream as a shear front or columnar disturbance mode (McEwan and Baines, 1974; Wei, Kao and Pao, 1975; Baines, 1977), so that the flow is subcritical in the hydraulic sense. R has the character of an inverse Froude number. The equations of motion may be rendered dimensionless by taking U as velocity scale, D/π as length scale, and $D/\pi U$ as time scale. Following McIntyre, we assume that the solution may be expanded in a power series in the small parameter $\varepsilon = \pi h/D$; the first term in this expansion then gives the linear solution. The corresponding equations in dimensionless form are given in the Appendix, together with the solution obtained by McIntyre's procedure in a form which is suitable for numerical evaluation for comparison with specific experimental cases. It should be noted that, as for Long's model (Davis, 1969; Baines, 1977), the solution (in the limit $t \to \infty$) for ψ and u diverges like $(K^2 - n^2)^{-1/2}$ as $K \to$ any integer n ($\neq 0$). Throughout this paper the same symbols x, z, t, ψ, and u, etc. are used to denote both the dimensional and dimensionless variables; apart from the Appendix the dimensional form is implied unless it is specifically stated otherwise.

It is interesting to evaluate representative values of K, R and ε for the atmosphere and ocean and to compare these with the experimental values. In this study the latter are in the range $0 < K < 3$, $0 < \varepsilon < 0.7$). For the atmosphere we take $D = 10$ km (tropopause height), $N = 10^{-2}\,\mathrm{s}^{-1}$, and we then have $K \sim 1$ for $U = 30$ m/s and $K \sim 3$ for $U = 10$ m/s. Values of R and ε for representative values of h are given in Table 1. It is seen that the experimental values are in the same range as those for typical

Table 1

$N = 0.01\ \mathrm{s}^{-1}$		$U = 10$ m/s	$U = 30$ m/s
		$K = 3.18$	$K = 1.06$
$h = 1$ km	$\varepsilon = 0.31$	$R = 1.0$	$R = 0.33$
$h = 3$ km	$\varepsilon = 0.94$	$R = 3.0$	$R = 1.0$

atmospheric situations. For topography on the ocean floor, if we take $D = 4$ km, $N = 10^{-3}$ s^{-1}, and $U = 10$ cm/s we have $K = 12.7$. Smaller values of K may be obtained with shallower depths, for example over continental shelves.

The plan of the paper is as follows. In section 2 details of experimental apparatus, methods and conditions are discussed. In sections 3 and 4 a detailed quantitative comparison between the observed flow fields and the linear theory is presented, for a wide range of the parameters R and K, and in section 5 the conclusions are summarized and their implications discussed. Broadly speaking, the observed supercritical flows ($K < 1$) are well-described by the linear theory in the parameter range investigated ($R \lesssim 0.8$). For the subcritical flows with $1 < K < 2$, the observed properties of the lee waves are generally consistent with the linear theory but, in many cases, flows over and upstream of the obstacle show significant differences from it, and this indicates that non-linear effects can be significant, even for small values (~ 0.1) of R.

2. Experimental apparatus and procedure

The experiments were carried out in the same tank as used in the experiments described in Baines (1977), except that it had been lengthened by inserting two glass-sided sections in the middle, giving a total length of 9.17 m and a width of 0.23 m. The tank was filled with a salt-stratified solution with a constant density gradient, using the customary two-tank method, to depths which varied from 0.18 m to 0.36 m. Fluid motion was generated by towing an obstacle at constant speed starting from rest along the bottom of the tank. The direction of towing was from right to left, as seen by the observers, and the starting position was situated approximately 1 m from the right-hand end of the tank. The fluid motion was visualized by means of neutrally buoyant expanded polystyrene beads, with a range of densities covering that of the fluid in the tank (typically 1.0–1.03 g/cm^3).

For each run, the flow was recorded by four cameras situated as shown in Fig. 1. Three stationary cameras, denoted by C1 to C3, were arranged along the tank and the fourth camera (denoted by C4) was located on a trolley which travelled along the tank with the obstacle and was

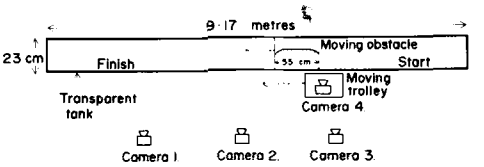

Fig. 1. Schematic plan of the experimental layout, with a long obstacle.

situated slightly behind it. The flow was illuminated from below through the transparent bottom by fluorescent lights which were collimated so as to illuminate the central region (spanwise) of the tank. The flow field immediately over the obstacle was illuminated by a fluorescent light suspended overhead which travelled along the tank with the obstacle and was supported from the trolley. The three stationary cameras gave a check on the constancy of the towing speed, showed the development of the flow as the obstacle travelled down the tank, and provided a clear picture of the flow around the obstacle. The fourth (moving) camera observed the development of the flow in the lee of the obstacle and permitted the measurement of the amplitude, phase and wavelength of the waves. With this arrangement the view of the flow field immediately behind the obstacle from cameras C1, C2 and C3 was partially obscured by camera C4 and the trolley framework as they passed, but this was not sufficient to seriously impair the flow visualization.

Four obstacles were used in the experiments, and these are listed and described in Table 2. Two of these obstacles (M1 and M2) are long, in the sense that they are somewhat longer than the depth of the fluid, and two (M3 and M4) are short. Several runs (a minimum of 10) were made with each obstacle, covering a range of flow conditions.

Table 2

Obstacle Number	Height h	Length 2a	Shape
M1	2.6 cm	55.0 cm	semi-ellipse
M2	1.1 cm	55.0 cm	flat, tapering to zero within 3 cm of each end
M3	3.1 cm	6.2 cm	semi-circle
M4	1.05 cm	2.10 cm	semi-circle

The procedure for each run was as follows. After the obstacle commenced motion, cameras C1, C2 and C3 all took time exposures at regular intervals, mostly of 2 or 3 s duration every 5 s, whilst C4 took $\frac{1}{2}$-s exposures at various positions along the tank. Synchronized clocks with "second" hands clearly visible were included in the fields of view of all cameras. The resulting set of "streak" photographs gave an almost complete description of the two-dimensional flow field, and all the results of this study were obtained from the examination of these photographs. Quantitative measurements of fluid velocity were obtained by measurements of streak lengths (or more precisely, length minus width).

Several runs were made with each tank filling. This was felt to be justified because the flow conditions were such that no instability and consequent mixing occurred in the internal wave field, although in some cases, particularly for the semicircular obstacles, there was a certain amount of separation and turbulence in the lee of the obstacle (described in more detail in sections 3 and 4). This resulted in some mixing and weakening of the density gradient up to a height which was approximately equal to that of the obstacle, and this effect accumulated as more runs were made. However, in all cases studied, this low-level mixing produced no observable change in the motions in the stratified fluid above. After the completion of each run, the fluid was allowed to rest until all fluid motion had decayed, before a new run was commenced. This required a minimum time of approximately 30 min between runs.

Towing speeds ranged between 4 and 12 cm/s, so that Reynolds numbers based on the height of the obstacle were in the range $400 < \mathrm{Re} < 3700$, where $\mathrm{Re} = Uh/\nu$. These towing speeds were too fast for the development of upstream boundary layers of the kind described by Martin and Long (1968). Hence boundary layer thicknesses on the top, bottom (upstream of the obstacle) and side walls may be characterized by $(\nu t)^{1/2}$, where t is the time elapsed since motion commenced at the point in question, and ν is the kinematic viscosity. Total towing times were mostly less than 150 s; most quantitative measurements were made with photographs from C1 and C2 where $t < 100$ s, so that $(\nu t)^{1/2} \lesssim 1$ cm. This distance is small compared with the depth and width of the tank, so that these boundary layers had a negligible effect on the main features of the interior flow. One aspect of the lower boundary should be noted here: the wire towing the obstacle ran along the centre of the bottom of the tank, and the drag of this wire generated velocities of considerable magnitude (but $< U$) in the adjacent fluid (within ~ 1 cm). Hence fluid measurements in this region were avoided.

The boundary layer on the obstacle itself is more significant. The structure of the flow outside the boundary layer varies considerably with the parameter K and also with position along the obstacle. However, the general features of this boundary layer will be similar to those of the corresponding boundary layer on a flat plate (for the long obstacles at least), and we will use this as a model. For the flat plate, the displacement thickness δ of the boundary layer is given by $\delta = 1.72(\nu x/U)^{1/2}$, where x is the distance from the leading edge. For the short obstacles M3 and M4 this gives a contribution to the effective obstacle height of order 1 mm, which we will neglect in the following sections, but for the long obstacles the thickness is larger. For an extreme case of $U = 4$ cm/s at the mid-point of the obstacle we have $x = 27.5$ cm, $\delta = 0.45$ cm, and at the end where $x = 55$ cm, $\delta = 0.64$ cm. This represents a significant contribution to the effective obstacle heights, particularly for the smaller obstacle M2. In view of the variability of the boundary layer properties and the other uncertainties in making observations of the fluid velocity from streaks, etc., I decided to base the correction to the effective obstacle height on the boundary layer thickness in the middle of the obstacle for both M1 and M2. We therefore have an effective obstacle height h_e defined by

$$\left.\begin{aligned} h_e &= h + 1.72\left(\frac{\nu a}{U}\right)^{1/2}, && \text{for M1, M2} \\ &= h, && \text{for M3, M4} \end{aligned}\right\}, \quad (2.1)$$

where a is the obstacle half-width. The viscous term increases the effective height by 3 or 4 mm. For theoretical calculations of lee waves, etc. the length and shape of the obstacles will be assumed to be unchanged, i.e. they will be taken as given in Table 2.

As far as could be judged from the photographs, the flow field was everywhere two-dimensional in all cases reported here, expecting in the low-level regions of separation and turbulence in the lee of the obstacle, where these occurred.

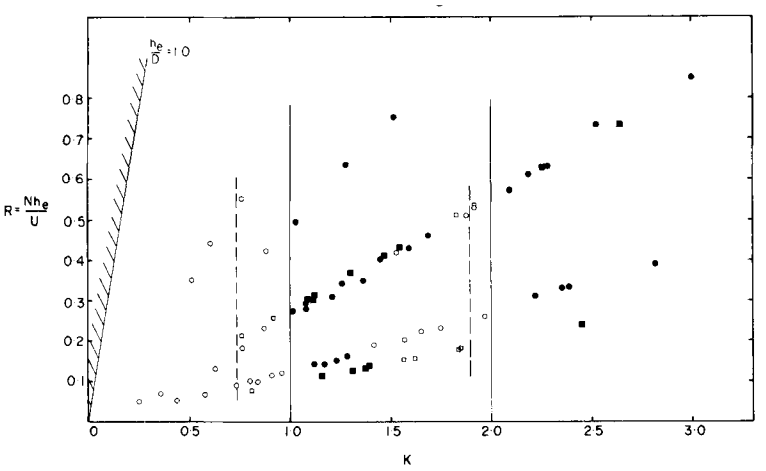

Fig. 2. Parametric values used in the present study. Each point denotes an experimental run, with the effective obstacle height h_e including the boundary layer displacement thickness (eq. 2.1). Circular points ○ ● denote long obstacles (M1, M2) and square points □ ■ denote short obstacles (M3, M4). Filled points ● ■ denote flows with upstream columnar motion attached to the obstacle at the end of the run. The vertical dashed lines at $K = 0.75$ and $K = 1.9$ denote the observed boundaries of the regions where the lee-side transient for the appropriate supercritical mode has not yet detached from the obstacle by the end of the run.

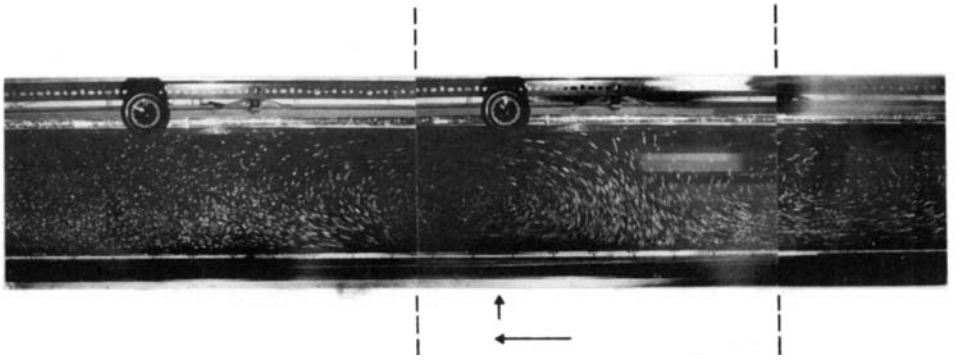

Fig. 3. A composite flow picture made from a sequence of frames taken by camera C1, showing the flow for $K = 0.96$, $R = 0.12$ with obstacle M2. Vertical dashed lines indicate the junctions of the frames. The vertical arrow denotes the centre of the obstacle, and the horizontal arrow its direction of movement. Time exposures are 2 s as shown by the clocks. The imposition of the moving carriage between camera C1 and the tank affects the right-half of the picture, but the transient lee-wave motion can be clearly seen and has not yet detached.

3. Supercritical flow—$K < 1$

We first consider flows for which $K < 1$, so that the flow is supercritical with respect to all linear wave modes. Conditions for the actual runs are represented by points in Fig. 2. The flows observed in the channel at the end of each run fall into two categories. In the first group the flow pattern in the immediate vicinity of the obstacle was steady and symmetrical about the centre line (as seen by camera C1), and this motion was followed, at a distance which increased with time, by a tadpole-like wave motion whose leading part considered of an "eddy" of comparable magnitude but reversed sign to the flow over the obstacle. Flows with these properties are represented by points to the left of the dashed line in Fig. 2 ($K < 1$). In the second group the flow over the obstacle was not quite symmetrical and was immediately followed by the "eddy" with reversed circulation, so that the two

were not separated. Flows of this kind are represented by points to the right of the dashed line ($K < 1$) in Fig. 2, and an example is given in Fig. 3.

According to the time-dependent linearized flow theory, as K approaches unity (or any other integer), the time taken for the flow to reach a steady-state near the obstacle increases without limit. Also, as discussed in the introduction, the theoretical expressions for ψ and u obtained from both Long's model and the linearized theory increase without limit like $(1 - K^2)^{-1/2}$, and consequently one expects these models to be inapplicable if $|1 - K|$ is sufficiently small. Solutions obtained from Long's finite amplitude model show that, if the flow far upstream is undisturbed by the presence of the obstacle (i.e. $\rho u^2(z)$ effectively constant), the steady-state flow pattern over a symmetrical obstacle must be symmetrical and have the character of the observed flows in group 1. It follows that if Long's model is to be inapplicable for some values of $K < 1$, the flow over the obstacle must generate a non-linear motion which propagates to upstream infinity at a supercritical speed, in a similar manner, perhaps, as that for one and two-layer flows (Houghton and Kasahara, 1968; Houghton and Isaacson, 1970; Long, 1970, 1974). It follows that the flows observed in group 2 could not yet have reached steady state, and there are two possibilities: either (i) the motion on the lee side eventually detaches and becomes transient, so that the flows evolve to the same state as those in group 1, or (ii) the motion over the obstacle generates a non-linear motion which propagates to upstream infinity at a supercritical speed.

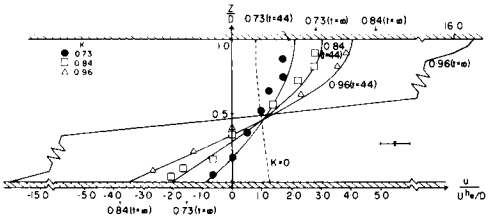

Fig. 4. Horizontal vertical profiles over the mid-point of the obstacle M2 for three supercritical flows $K = 0.73$, 0.84 and 0.96. The experimental values for the dimensionless time $t = 44$ as seen by camera C1 are compared with the corresponding profiles obtained from linear theory. The theoretical profile for $t = \infty$ for $K = 0.96$ is also shown, and the end points for $K = 0.73$, 0.84 are indicated by arrows. The dashed line shows the corresponding profile for potential flow ($K = 0$).

For all runs in group 2 the flow fields seen by cameras C1 and C2 were carefully compared for any evidence of a build-up of fluid on the upstream side as the genesis of an upstream wave, but no change of flow field on the upstream side between C1 and C2 was detected. The observed flow fields were then compared with those obtained from time-dependent linear theory (see Appendix), and it was found that the observed position of the downstream eddy was quite compatible with linear theory in every case for flows in both groups 1 and 2. The theoretical distance between the obstacle and eddy increases at the dimensionless rate of $1 - K$. This strongly suggests that, for the flows studied, the lee-side motion is detaching and becoming transient and that the boundary in Fig. 2 between groups 1 and 2 moves steadily to the right as the length of the run increases. In other words, all flows in group 2 evolve to the same state as those in group 1, and the process is adequately described by linear theory. Convincing evidence that this is so is presented in Fig. 4. Here, velocity profiles observed by C1 over the centre of the obstacle for three cases $K = 0.73$, 0.84 and 0.96 for obstacle M2 are compared with their theoretical values obtained from linear theory for the actual length of run (dimensionless time $t = 44$ for all three cases). For all cases the agreement is quite good. The end points of the theoretical profiles when $t = \infty$ are indicated with arrows, and their shapes are stretched versions of those for $t = 44$. The $K = 0.96$ flow in particular, requires much more time to attain steady state, where the fluid velocities would be much larger.

Hence, for all runs studied, which cover K values up to 0.96, the flow appears to be adequately described by linear theory, and *ipso facto* by Long's model for the steady state, although quantitative comparisons with the latter have not been made here. The question then arises, how close must K be to unity for the flow field to depart significantly from linear theory and Long's model? A partial answer to this question is suggested by the work of Su (1976) who obtains criteria for the existence of hydraulic jumps in a continuous stratification of finite depth. If hydraulic jumps are *possible* for a given supercritical state they will provide a means of propagating disturbances upstream at supercritical speed, which is necessary for the amelioration of the consequences from Long's model as $K \to 1-$. Su's work is based on

Table 3

βD	Ranges of K for which internal hydraulic jumps are possible		
1.686	$0.9856 < K < 1.0$	$1.9997 < K < 2.0$	$2.9994 < K < 3.0$
0.1686	$0.9998 < K < 1.0$	$1.999998 < K < 2.0$	$2.99994 < K < 3.0$

momentum and energy considerations which have been used with success in layered flows and gas dynamics. He takes the density profile to be $\rho = \rho_0 e^{-\beta z}$ and assumes that the flow is hydrostatic and that the jump is moving into undisturbed stationary fluid. The appropriate dimensionless parameters are K and βD—a measure of the total density variation. Su gives numerical results for two values of βD and finds that, under these conditions, internal hydraulic jumps are only possible for the ranges of K given in Table 3.

For the experiments described in this paper $\beta D \sim 0.03$, so that the permissible ranges of K would be even narrower (if they exist at all). Hence there would be no possibility of observing such hydraulic jumps in experiments of this nature, even with tanks much longer than that used in these experiments, although a continuous flow apparatus with very accurate speed control may be successful.

4. Subcritical flow—$K > 1$

Conditions for the various subcritical runs are shown in Fig. 2 for $K > 1$. The observations have been concentrated in the region $1 < K < 2$, in order to obtain a complete description of the properties of the first mode, but some observations with $K > 2$ were also made.

Observed flow patterns in the vicinity of the obstacle as seen from the stationary camera C1 are shown in Fig. 5, for three sequences of runs. These are for three different obstacle shapes and a range of values of K, the latter being varied in each sequence by changing the towing speed U. Each sequence of flow patterns shows the same general character. As K increases through unity, the "eddy" which is situated over the obstacle for $K < 1$ begins to elongate and extend on the upstream side, where it has a sinusoidal mode 1 structure in the vertical. The front of this motion propagates upstream at a speed which is difficult to measure accurately but is generally slightly less ($\sim 10\%$) than the linear long wave speed (ND/π) for the first mode. No systematic variation in this speed with R or K could be detected. This "eddy" is terminated on its near side by a narrow region of descending motion which moves from the rear of the obstacle toward its front as K increases above unity. For all run sequences in these experiments, a value of K (<2) is eventually reached at which this upstream "eddy" separates from the obstacle and propagates ahead of it leaving an intervening space with no detectable motion. After this has occurred the flow pattern over the obstacle has a dominant mode 2 structure. Downstream of the obstacle lee waves of the familiar type are observed, and these are discussed in more detail below.

The horizontal velocity in the upstream motion may be written

$$\frac{u}{U} = u_1(x, t) \sin \frac{\pi z}{D}, \tag{4.1}$$

and as the "eddy" passes, the amplitude u typically rises to a maximum and then decreases to a steady value before the obstacle is reached or, if the motion has detached, it falls to zero. Values of these maxima and steady state amplitudes of u/U are given in Fig. 6a for long obstacles and Fig. 6b for short obstacles. For K near unity, no values were recorded if u/U was still increasing at the front of the obstacle. The open circles and squares denote points where the upstream "eddy" has become detached from the obstacle, so that the steady state value is (apparently) zero. Lines of constant amplitude *suggested* by the point values are sketched on the figures, and these are included to show the general pattern of the results. In Fig. 6a an open point exists at $K = 1.54$, $R = 0.43$, indicating a detached upstream "eddy". However, there are indications that the upstream motion is being re-established immediately ahead of the obstacle (Fig. 5a frame 5), so that this point is not regarded as being inconsistent with the general pattern. Provided K is not too close to unity (i.e. K lies outside the range $1 < K \lesssim 2$) or 2, 3, etc. the flow pattern over the obstacle is essentially un-

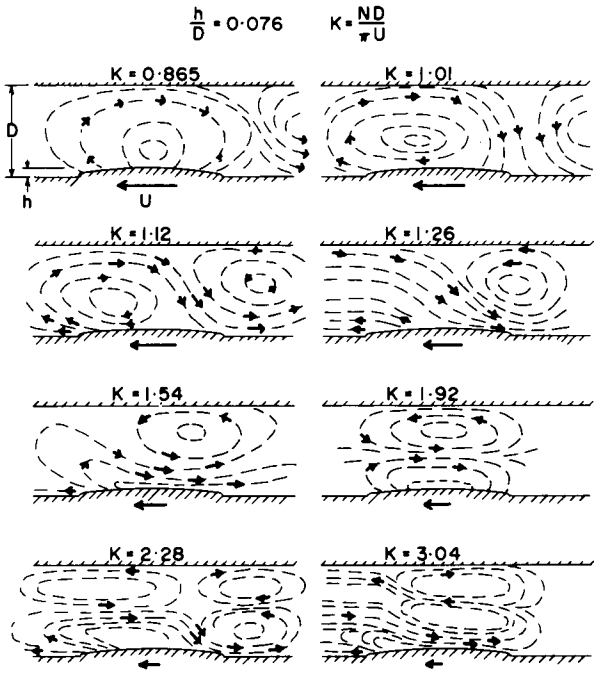

Fig. 5a. Instantaneous flow patterns over the obstacle M1 as observed by the stationary camera C1, for various runs with $h/D = 0.076$. The lengths of the arrows (but not the other streaks) indicate velocity magnitudes, relative to the obstacle speed U, which is shown below each figure.

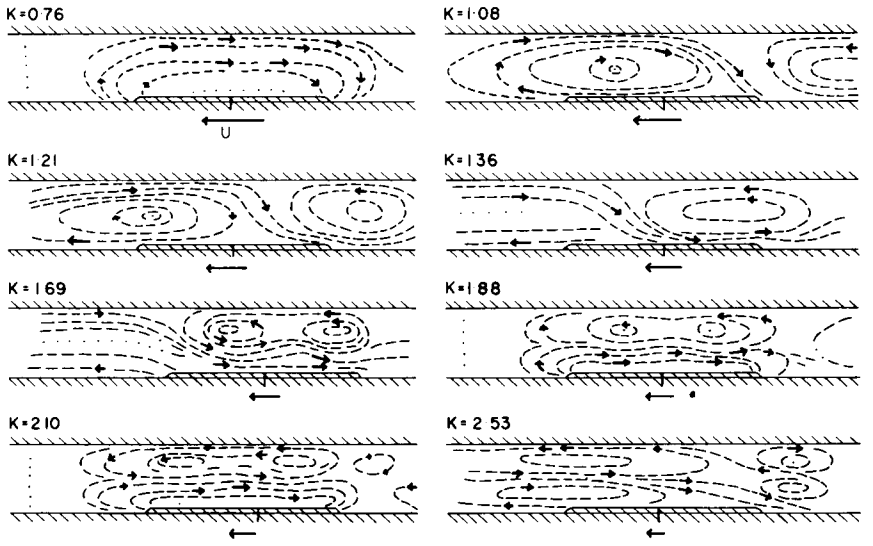

Fig. 5b. As for Fig. 5a but for obstacle M2 and $h/D = 0.059$.

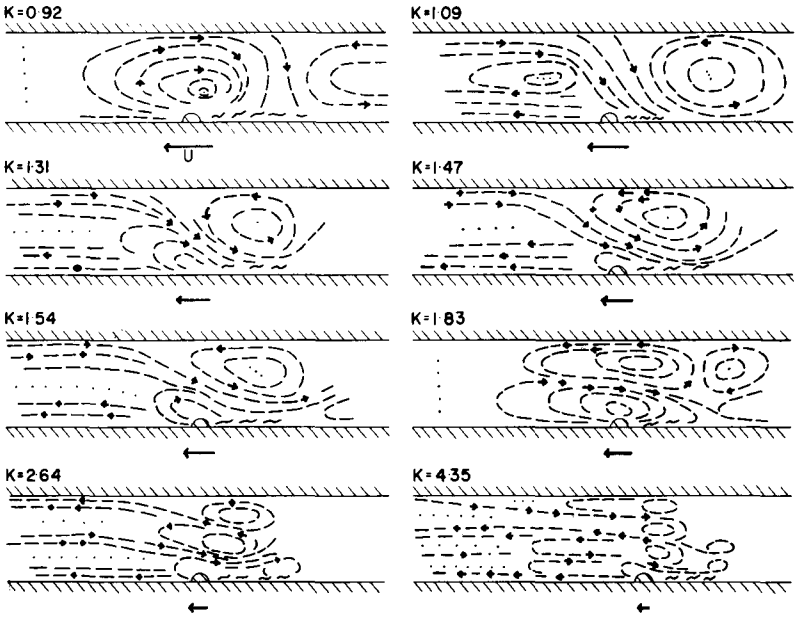

Fig. 5c. As for Figs. 5(a), (b) but for obstacle M3 and $h/D = 0.089$.

changed from C2 to C1, indicating that an approximately steady state has been obtained in this region.

We next compare this observed motion upstream and over the obstacle with the predictions of the linear model, again using the equations given in the Appendix. For this purpose we will concentrate on one particular sequence of runs, namely that shown in Fig. 5b. This has been chosen because it gives a good coverage of the range $1 < K < 2$, and has the largest dimensionless time value at C1 ($\pi Ut/D \sim 90$ when the obstacle arrives) of all the sequences. Fig. 7 shows a comparison between the linear theory and the observed flow for the upstream motions, where the quantity plotted is the magnitude of the horizontal velocity near the upper boundary, suitably scaled, as a function of x for $T = \pi Ut/D = 83.0$. Since camera 1 has a limited field of view, for the larger values of K the observational curve must be constructed from a sequence of pictures taken at different times with $T < 83$. The curve at $T = 83$ was then obtained by placing the leading part or nose of the motion at a position consistent with its observed speed of propagation, and "stretching" the curve by a factor proportional to its distance from the obstacle so as to fill up the complete range between the nose and the obstacle. The curves obtained from the linear theory consist of an initial hump or maximum—which corresponds to the transient term described above for $K < 1$, only it now appears upstream, and this is followed by a decaying oscillating tail which is adequately described by a stationary phase approximation to the transient part of the (Cauchy principal value) integral A13. At a fixed distance upstream of the obstacle this oscillating motion is $O(1/t^{1/2})$ for large t. The contrast between the observed motion and predictions of linear theory is quite striking, for all values of K.

As another quantitative comparison for these six runs, we examine the horizontal (at $x = 0$) and vertical (at mid-depth, $z = D/2$) velocity profiles over the obstacle. These are shown in Fig. 8 for $\pi Ut/D = 90.0$. For $K = 1.08$, 1.21 the difference between linear theory and observation is very marked, for both the u and w profiles. However, as K increases the difference between the two sets of profiles progressively decreases, for both u and w. Together these sets of comparisons (Figs. 7 and 8) show that, for $\varepsilon = \pi h_e/D = 0.25$ (the small parameter in McIntyre's expansion), the observed flow upstream and over the obstacle departs significantly from that predicted by linear theory, and this difference is generally larger the closer K is to

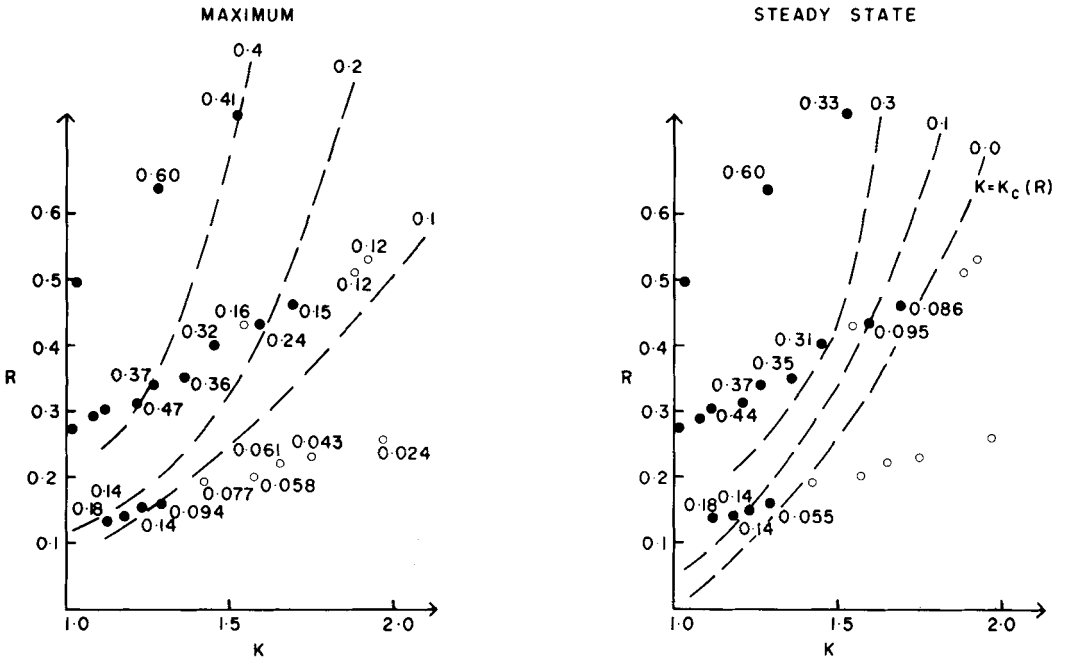

Fig. 6a. Maximum and steady-state values of the upstream amplitude function u_1 (eq. 4.1) of the horizontal velocity for the runs with long obstacles (M1 and M2), measured near the upper surface ($z = D$). Lines of constant amplitude suggested by these point values are shown dashed, and the line where the steady-state value has fallen to zero is denoted $K = K_c(R)$. Accuracy of the point values is estimated to be ±10%. The symbols have the same meaning as in Fig. 2.

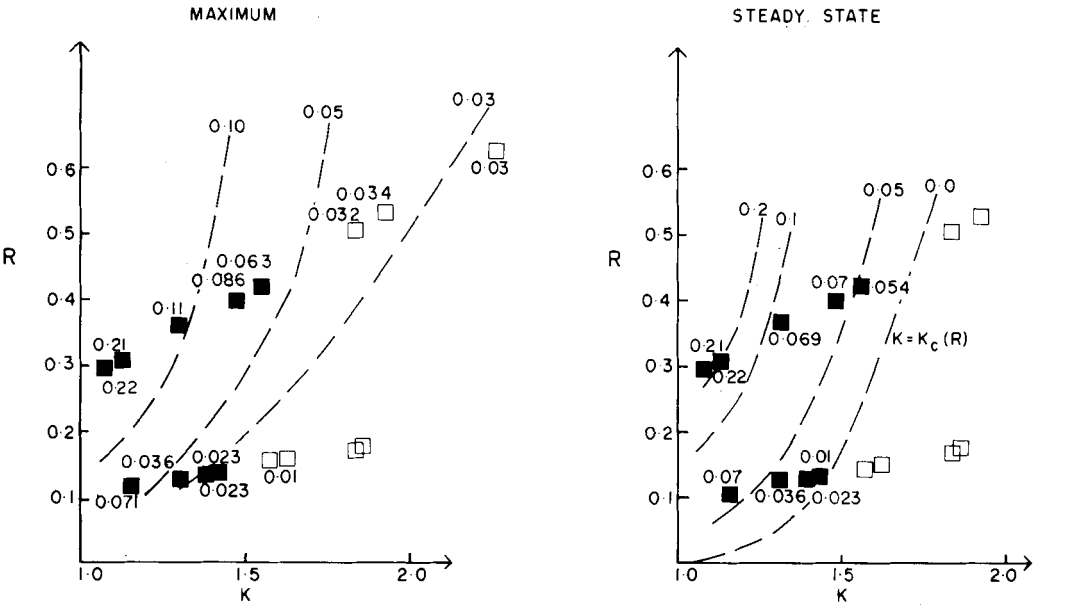

Fig. 6b. As for Fig. 6(a) but for the short obstacles M3 and M4.

unity. As K increases above unity, a point is reached where, although the transient behaviour still differs, the steady state (or larger time limit) behaviour is similar. Although quantitative comparisons have not been made, a similar contrast is apparent for each of the other sequences of runs, for both the long and the short obstacles, with values of ε down to 0.094. The same pattern of behaviour is also seen for mode 2 when $K > 2$, although mode 2 has not been observed to detach upstream. Two visual examples in the form of composite photographs taken by C1 are shown in Fig. 9.

We next discuss the lee waves and downstream properties. The linearized theory predicts a lee wave train of dimensionless length $(1 - 1/K^2)t$. For K close to unity this distance is very short, but for $K \gtrsim 1.2$ lee waves were observed and measureable, and the length of the wave train was seen to be generally consistent with linearized theory. A comparison between observed and theoretical lee wavelengths for all series of runs is shown in Fig. 10. There is some scatter, but the agreement is generally good, and no significant departure from linear theory can be detected. We next consider lee wave amplitudes and phases. These are a function of obstacle shape, and they cannot all be plotted on a single diagram. It is necessary to compare theory and observation for each series of runs separately, and this is done in Fig. 11 for the long obstacles and in Fig. 12 for the short obstacles. For each wave mode the amplitude ζ_a and phase ϕ are defined by

$$\zeta = -\zeta_a \sin(kx - \phi) \sin n\pi z/D, \tag{4.2}$$

where ζ denotes vertical displacement from the equilibrium position and $\zeta_a > 0$, so that a wave has zero phase if its point of maximum downward velocity (at mid-depth for mode 1, $D/4$ above bottom for mode 2) is situated over the mid-point of the obstacle. In fact the phase was actually measured at points downstream of the obstacle, where the wave was more clearly defined. For the long obstacles the amplitudes generally agree quite well with the predictions of linear theory, but the phases are somewhat scattered, particularly when K is larger than the first zero of the amplitude function. The jump of π in phase in the theoretical curves is caused by the amplitude changing sign—for the obstacle M1, for example, it has Bessel function behaviour. There is a tendency for the phases to be more in agreement with the linear theory as h/D decreases.

Results for the short semi-circular obstacles, shown in Fig. 12, contrast with those for the long obstacles, in that the phases are now in satisfactory agreement but the observed amplitudes significantly exceed the theoretical ones. This discrepancy may be attributed to the separation that occurs on the lee side of the obstacle, which increases its effective length. The subject of separation behind obstacles in stratified fluids is complex and little-studied. In the present experiments, the separation region for M3 could be clearly seen (Fig. 13a), and the observed length of the separation region decreased with increasing K (decreasing U) from ~23 cm for $K = 0.76$ ($U = 11.5$ cm/s) to ~10 cm for $K = 1.92$ ($U = 4.55$ cm/s). These correspond to Reynolds numbers in the range $1410 < \mathrm{Re} < 3560$. For the smaller obstacle M4 a corresponding separation region appeared to be present but the flow visualization was inadequate for quantitative measurement. A comparison of the observed lee wave amplitudes with theoretical ones obtained using an obstacle shape which approximated that of the obstacle plus the finite separation region gave generally better agreement, as indicated by the dashed curve in Fig. 12a (where a constant obstacle length has been used), and this was accompanied by only a small change in phase.

It is well known (Trustrum, 1964; Wong and Kao, 1970) that an obstacle which exhibits "source-like" behaviour in a stratified fluid generates upstream motions which are essentially the same as those described here, according to linear theory. Wei et al. (1975) observed this type of upstream motion, which they termed "columnar disturbance modes", using very bluff obstacles (vertical barriers and circular obstacles). They attributed this upstream motion to the presence of a growing turbulent separation region downstream which, they suggested, caused the obstacle to have source-like behaviour for the purposes of the internal wave motion. This possibility was examined for the present series of experiments, and two representative photographs of the flow on the lee side of the obstacles, taken by camera 4 when near the field of camera 1, are shown in Fig. 13. As described above, behind the semi-circular obstacle (Fig. 13a) there is a finite separation region, and after the flow is established this remains constant in length. The region following this separation region,

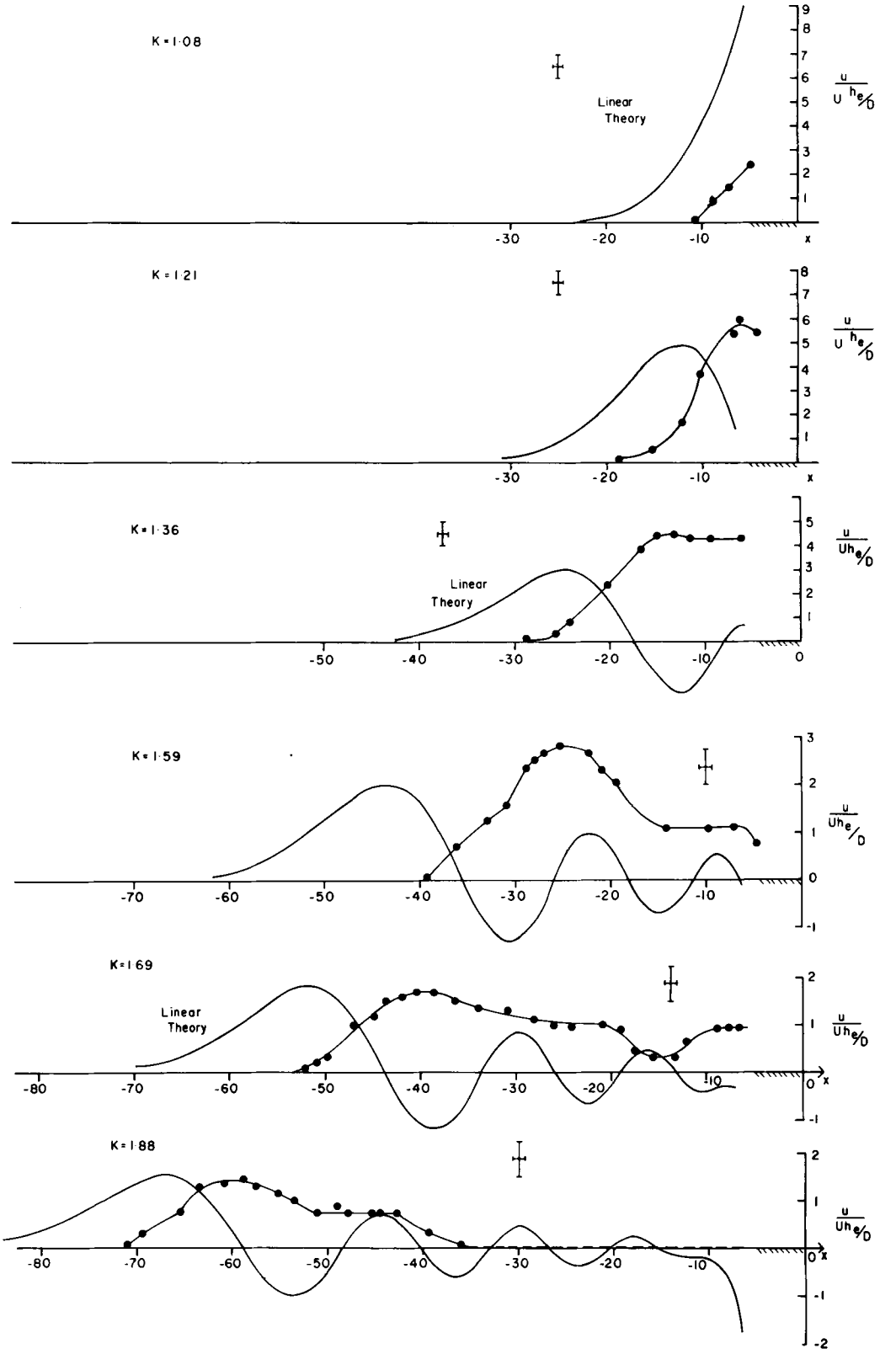
K = 1·08
Linear Theory
K = 1·21
K = 1·36
Linear Theory
K = 1·59
K = 1·69
Linear Theory
K = 1·88

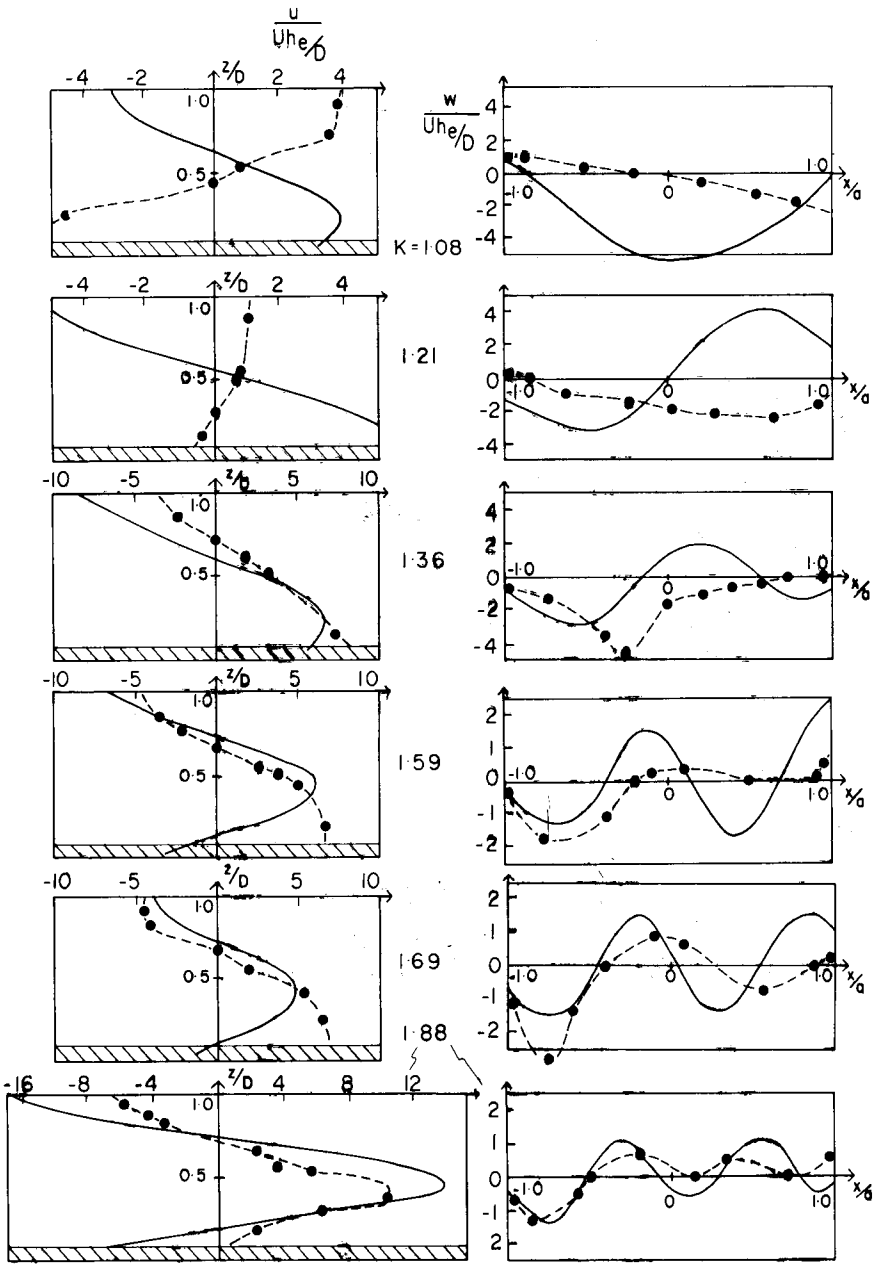

Fig. 8. Horizontal velocity profiles over the centrepoint ($x = 0$) and vertical velocity profiles at mid-depth ($z = D/2$) for the obstacle M2 at time $\pi Ut/D = 90.0$, for the same set of runs as in Fig. 7. The points denote the observations, and the continuous lines the corresponding predictions from linear theory. Observational accuracy is ±10%.

Fig. 7. Upstream horizontal velocity u observed near the top boundary, compared with the corresponding predictions of linear theory, for obstacle M2 with $h/D = 0.059$, for dimensionless time $\pi Ut/D = 83.0$. Except when close to the obstacle, these waves represent the function u_1 of eq. 4.1 (apart from the nearly constant factor h_e/D). The horizontal scale is in units of D/π

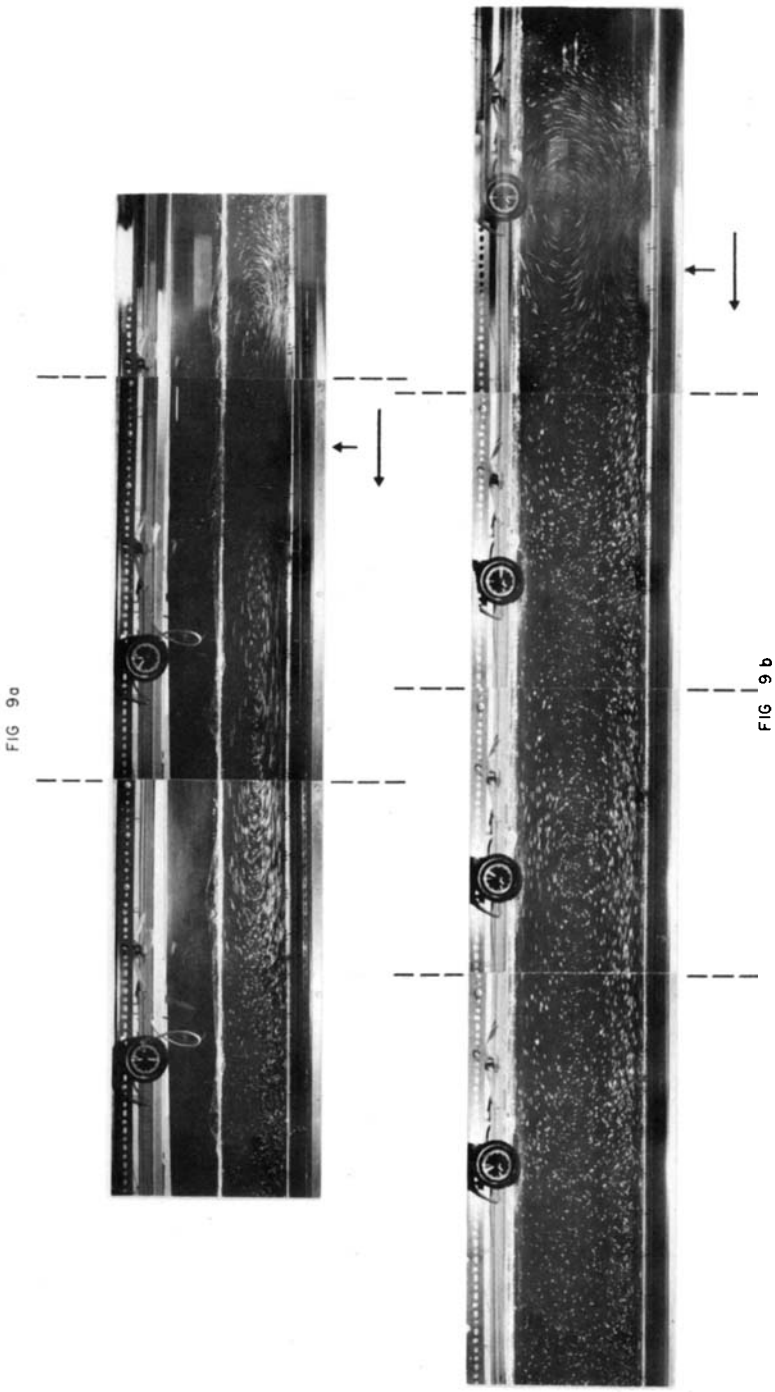

Fig. 9. Composite photographs for two runs, each constructed from a sequence of pictures taken by camera C1. (a) Obstacle M2 with $h/D = 0.059$ and $K = 1.36$; (b) Obstacle M3 with $h/D = 0.089$, $K = 1.47$. Vertical dashed lines indicate the junctions of the frames. Vertical arrows denote the centre of the obstacle, and horizontal arrows its direction of movement.

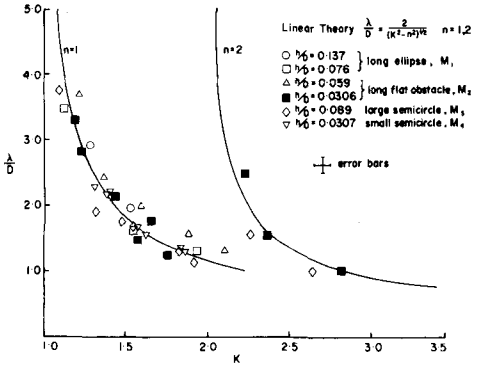

Fig. 10. The observed wavelengths of lee waves compared with linearized theory (solid curves), for all obstacles.

whilst not perhaps being perfectly laminar, is indistinguishable from the wavy fluid above, and there is no suggestion of a thin layer of fluid (turbulent or otherwise) following the obstacle. For the long obstacles, flow separation on the lee side was negligible for most cases, and a typical example is shown in Fig. 13b. It is clear from these and other photos that, for both the long and short obstacles, there is no growing separation region attached to the lee side of the obstacle which acts to increase its effective length, and hence cause the upstream motions described above.

5. Conclusions and Discussion

The main conclusions of this paper may be summarized as follows.

(i) For supercritical flows ($0 < K < 1$) with $\varepsilon = \pi h_e/D$ less than about 0.75, the time-dependent flow field observed is well described by linear theory within the time limit of the experiments ($\pi Ut/D \gtrsim 90$). The steady-state flow pattern consists of localized flow over the obstacle with clockwise vorticity (with flow relative to the obstacle from left to right), with transients containing opposite vorticity advected downstream. As K approaches unity the lee-side transient motion takes more time to detach from the motion over the obstacle, and the theoretical steady-state velocities increase like $(1 - K^2)^{-1/2}$, but no significant departure from linear theory could be detected, even with K values as large as 0.96.

(ii) For subcritical flows with $1 < K < 2$ and $0.1 < \varepsilon < 0.5$, the general properties of the observed lee wave field (mode 1 only)—namely its structure, wavelength, amplitude and phase—are in agreement with the theory to a reasonable degree of accuracy. For the long obstacles, the amplitudes are in good agreement whereas the phases show some scatter and a tendency to be slightly positive relative to the theoretical values (i.e. the wave is slightly displaced in the downstream direction). For the shorter semi-circular obstacles, the situation is complicated by the presence of a lee-side separation region with a length which is several times that of the obstacle. Here the observed lee wave amplitudes are much larger than those obtained from linear theory based on the obstacle shape, and it appears that it is more appropriate to take "obstacle plus separation region" as the theoretical obstacle in these circumstances, although this has not been checked in detail.

(iii) Whereas the lee wave field for subcritical flows is in reasonable agreement with the linear theory, the observed flow upstream and over the obstacle shows some substantial differences. Linear theory predicts wavy transient motion with mode 1 structure on the upstream side, propagating ahead of the obstacle and decaying like $1/t^{1/2}$ for fixed x and large t. The observed flow upstream has mode 1 structure with the (perturbation) flow away from the obstacle for $z < D/2$; its amplitude rises to an initial maximum and then falls to a constant value which persists until the obstacle is reached, if K is less than some value $K_c(R)$ (indicated in Fig. 6) which depends on R and, to a lesser extent, on the obstacle shape. If K is greater than this value $K_c(R)$ the upstream motion detaches from the obstacle and propagates ahead of it, leaving an intervening space with no detectable motion. Whether it detaches or not, this upstream motion never changes sign and is quite different from the wavy transients of linear theory. Its amplitude decreases with increasing K. Over the obstacle, the flow shows a corresponding large departure from linear theory when K is near (but greater than) unity, but theory and experiment generally become progressively more similar as K increases above unity. Similar behaviour is observed with the higher modes for larger K.

For $1 < K < K_c(R)$ the question arises as to whether the upstream motion remains attached to the obstacle for all time and extends to upstream infinity, or whether it ultimately detaches and becomes transient, like the cases where $K > K_c(R)$. Although the answer may be a mixture of both of

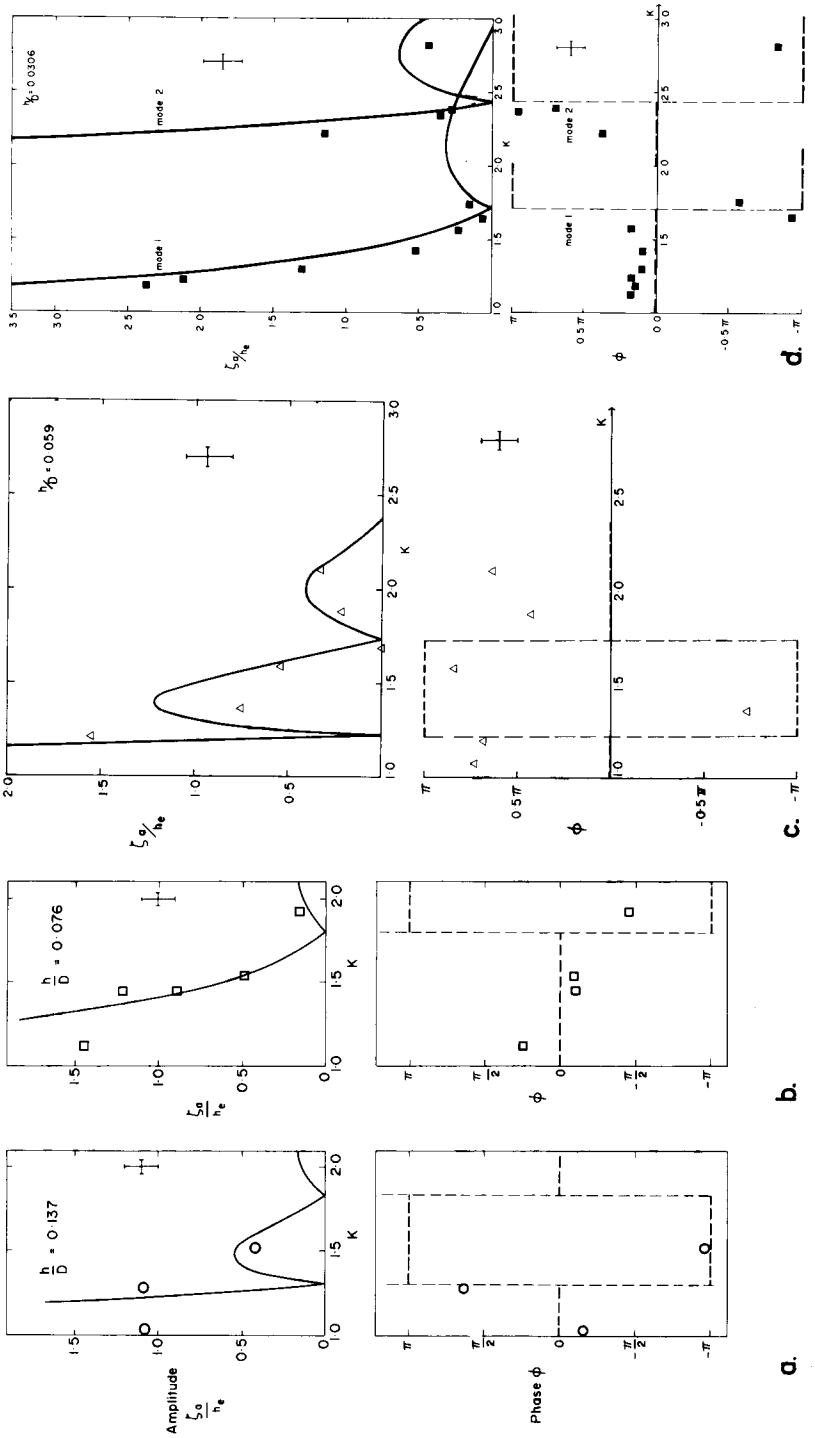

Fig. 11. Lee wave amplitudes ζ_a and phases ϕ for runs with the long obstacles M1 and M2, compared with the linear theory (solid curves). ζ_a and ϕ are defined by equation 4.2. (a) M1, $h/D = 0.137$; (b) M1, $h/D = 0.076$; (c) M2, $h/D = 0.059$; (d) M2, $h/D = 0.031$. For (d), when $K > 2$ the points refer to mode 2.

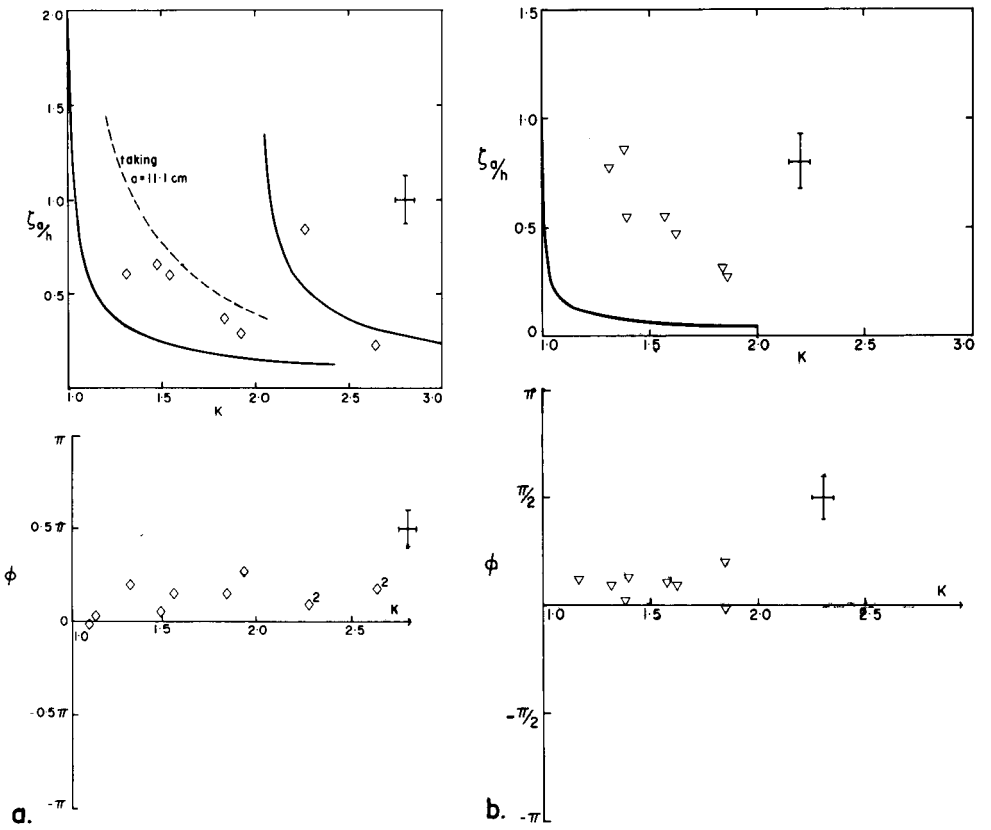

Fig. 12. As for Fig. 11 but for the short obstacles M3, M4. (a) M3, $h/D = 0.089$; (b) M4, $h/D = 0.031$. The dashed curve in Fig. 12(a) denotes the theoretical curve obtained by taking obstacle half width $a = 11.1$ cm. For $K > 2$ the points refer to mode 2.

these possibilities, it is felt that the upstream motion probably persists for most of the range $1 < K < K_c(R)$ for the following reasons. Firstly, for all relevant experimental runs there is no significant difference between the flow fields near the obstacle seen by cameras C1 and C2 (whereas there is between cameras C2 and C3), indicating that the local flow is an approximately steady state. Secondly, this type of motion is consistent with the motion observed with larger values of R and K by the author (Baines 1977), when such motion is obviously not transient, and it therefore provides a natural continuation into this parameter range. Thirdly, the singular behaviour of the linear theory at $K = 1$ implies the presence of non-linear effects for K sufficiently close to 1, regardless of how small h is (for inviscid fluids). This suggests that $K_c \to 1$ as $R \to 0$.

One important constraint of stratified flows of this kind is that the total area (or volume) below each line of constant density must remain constant. If a line of constant density is elevated above its mean position upstream, it must be depressed downstream. This implies that, if the upstream motion just described is to extend from the obstacle to upstream infinity, there must be a corresponding (but not necessarily sinusoidal) downstream motion extending to minus infinity to compensate. In the present experiments this compensating motion is visible over and immediately behind the obstacle for the long obstacles, but is scarcely visible for the short obstacles where the upstream motion is smaller. In other words, the downstream motion appears to be larger and extends more slowly than the upstream motion.

With regard to the steady-state ($t \to \infty$) flow, on the basis of the present experiments it appears that for $R \lesssim 0.7$, $\varepsilon < 0.7$ and $K < 2$ the ideal inviscid

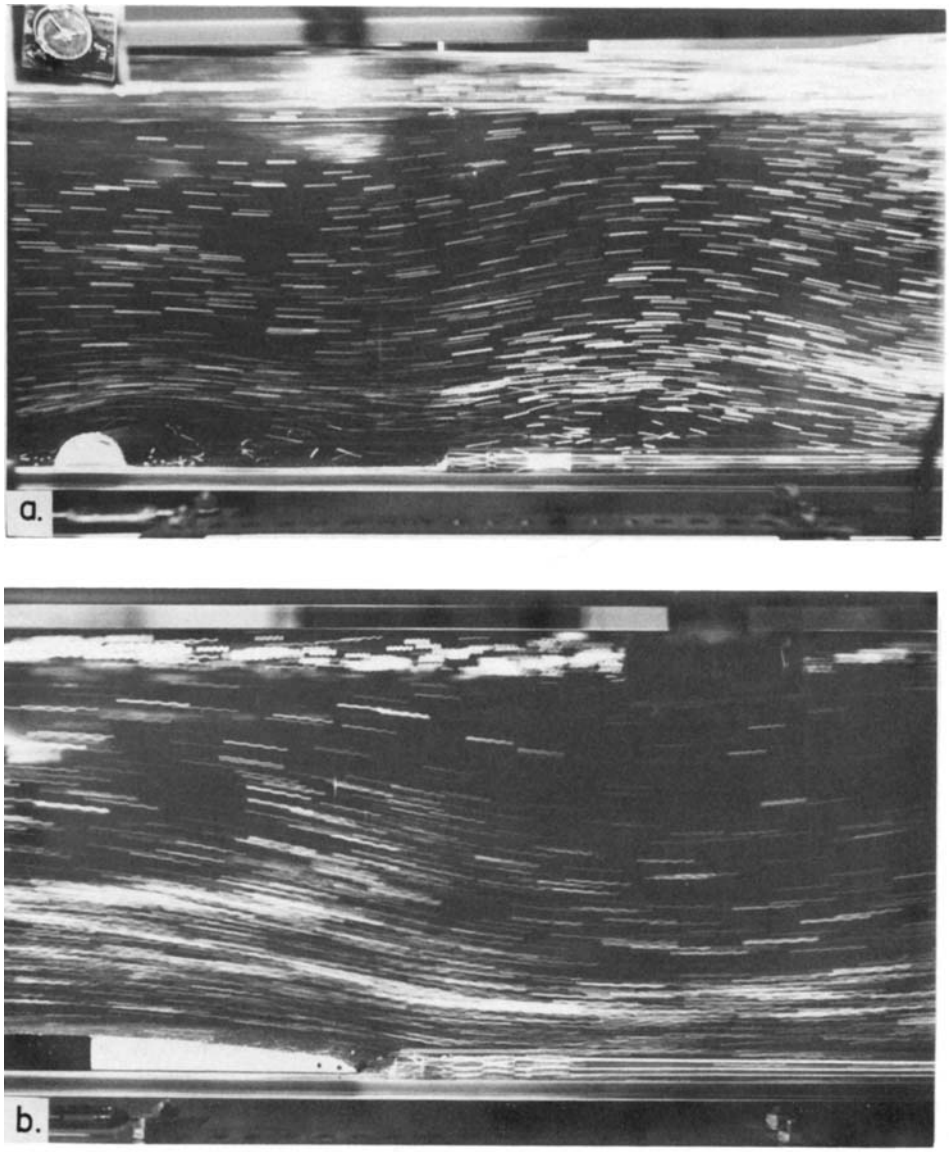

Fig. 13. Flow fields relative to the moving obstacle, photographed by camera C4. (a) M3, $h/D = 0.089$, $K = 1.47$; (b) M1, $h/D = 0.076$, $K = 1.12$.

flow would be well-described by Long's model for K in the range $0 < K < 1 - \delta_1$, $K_c(R) < K < 2 - \delta_2$, where δ_1 and δ_2 are unknown but probably very small numbers as discussed in Section 3. The best observational approximations to the function $K_c(R)$ are given by the curves in Fig. 6. For $\delta_1 < K < K_c(R)$ the flow is influenced by non-linear effects which cause disturbances to be sent upstream and downstream, altering the flow conditions at infinity in the limit $t \to \infty$. For $\delta_1 < K < 1$ the leading part of this upstream motion must also be non-linear, as it must propagate at a supercritical speed.

It should be noted that all of these conclusions apply to flows where the obstacle speed is increased suddenly from rest to a constant value. It is quite possible that there may be hysteresis effects in

some cases associated with the non-linear behaviour, so that the final steady-state may depend on the manner in which the external flow variables (notably U) approach their final values. In particular, the flow might approach the Long's model solution as $t \to \infty$ for $1 < K < K_c$ if the approach to steady state is appropriately chosen.

What is the nature of the breakdown of linear theory? In McIntyre's (1972) analysis, based on a perturbation expansion in powers of ε, the second-order terms are numerically much smaller than the first-order ones for the present experiments. Baines and Grimshaw (1979) have considered a different expansion with N/U as the small parameter and finite h, for the case of infinite depth. The results of that study are quite consistent with the small h expansion and Long's model, in that no permanent upstream effects are obtained. It therefore appears that the departures from linear theory observed in these experiments where $R \lesssim 0.7$ are directly attributable to the finite depth of the flow, and are related to the singularities of the linear solution at K = integer n. An examination of the linear solution for K exactly equal to n shows that the horizontal velocity with mode n structure grows without limit like $t^{1/3}$ for all x, for large t. This implies that non-linear effects must become important when $\varepsilon(\pi Ut/D)^{1/3} \sim 1$, and a non-linear model along these lines is currently being developed.

The flows described herein are for the special situation of constant stratification and finite depth, and the question arises, what relevance do they have for realistic flows in, for example, the atmosphere? Finite depth modes are analogous to trapped modes in the vertical in an unbounded and more general stratification. Hence the results presented here should be representative of the behaviour of vertically trapped modes in the atmosphere, particularly near their critical (maximum) speeds. These results also suggest the nature of the evolution of the flow with continuously changing stratification to that other limiting case of vertically trapped motion, a single interface.

6. Acknowledgements

I am very grateful for the enthusiastic cooperation of David Murray, George Scott and Ian Helmond with photography and numerous experimental matters.

7. Appendix

Equations for the computation of linearized time-dependent flow.

For the conditions of the experiments, the linear initial value problem in dimensionless form may be expressed as

$$\left(\frac{\partial}{\partial t} + H(t)\frac{\partial}{\partial x}\right)^2 \nabla^2 \psi + K^2 \psi_{xx} = 0, \tag{A.1}$$

$$\left.\begin{aligned} \psi &= 0 && \text{on } z = \pi, \\ \psi &= H(t)\, f(x) && \text{on } z = 0, \end{aligned}\right\} \tag{A.2}$$

where $H(t)$ denotes the Heaviside step function, $\varepsilon = \pi h/D$, and

$$\psi = 0, \qquad \text{for } t < 0. \tag{A.3}$$

The fluid velocity is given by

$$u = 1 + \psi_z, \qquad w = -\psi_x. \tag{A.4}$$

These equations result from a formal expansion in powers of small obstacle height with the solution as the first term, and the reader is referred to McIntyre (1972) for details.

Provided that K is not an integer the solution to this problem (following McIntyre) is given by

$$\psi(x, z, t) = \int_{-\infty}^{\infty} e^{ikx}\, \tilde{\psi}(k, z, t)\, dk,$$

where

$$\tilde{\psi}(k, z, t) = \tilde{\psi}_s(k, z) + \tilde{\psi}^+(k, z, t) + \tilde{\psi}^-(k, z, t), \tag{A.5}$$

$$\tilde{\psi}_s(k, z) = -\tilde{h}(k)\frac{\sin\,(K^2 - k^2)^{1/2}\,(\pi - z)}{\sin\,(K^2 - k^2)^{1/2}\,\pi}, \tag{A.6}$$

$$\tilde{\psi}^{\pm}(k, z, t) = \sum_{n=1}^{\infty} \tilde{\psi}_n^{\pm}(k, t) \sin nz, \tag{A.7}$$

$$\tilde{\psi}_n^{\pm}(k, t) = \frac{nc_n^3\, \tilde{h}(k)\, e^{-ik(1 \pm c_n)t}}{\pi K^2 (1 \pm c_n)}, \tag{A.8}$$

$$\tilde{h}(k) = \frac{\varepsilon}{2\pi}\int_{-\infty}^{\infty} f(x)\, e^{-ikx}\, dx, \tag{A.9}$$

and

$$c_n = \frac{K}{(k^2 + n^2)^{1/2}}. \tag{A.10}$$

The path of integration lies along or slightly to either side of the real k-axis. The initial conditions

appropriate here differ slightly from those used by McIntyre, and this results in c_n^3 in eq. (A.8) instead of c_n^4.

If the obstacle is symmetric, as in these experiments, $h(k)$ is even and for $K < 1$ the solution may be expressed in the form

$$\psi = \psi_s(x, z) + \sum_{n=1}^{\infty} \psi_n(x, t) \sin nz, \tag{A.11}$$

where

$$\psi_s(x, z) = -2 \int_0^{\infty} \tilde{h}(k) \cos kx \cdot \frac{\sin (K^2 - k^2)^{1/2}(\pi - z)}{\sin (K^2 - k^2)^{1/2} \pi} dk, \tag{A.12}$$

$$\psi_n(x, t) = \frac{2K}{\pi} \int_0^{\infty} \frac{n\tilde{h}(k)}{(n^2 + k^2)^{3/2}} \times \left[\frac{\cos k(x - (1 + c_n)t)}{1 + c_n} + \frac{\cos k(x - (1 - c_n)t)}{1 - c_n} \right] dk. \tag{A.13}$$

In eq. (A.12), "sin" is replaced by "sinh" when $k > K$. These integrals may be readily evaluated numerically on the real axis for any x, z and t. The term ψ_s gives the steady state flow in the limit $t \to \infty$ in the vicinity of the obstacle. The other terms represent dispersing transients, the ψ_n^- terms being the most important as they are larger and represent motion propagating against the stream.

For $K > 1$ the integrands of ψ_s and (some of) ψ_n^- have poles on the real axis, and the contour must be taken around them, on either side but the same for each integral. The sum of the pairs of semi-residues is zero, so that one is left with the Cauchy principal values of these integrals, and these may also be evaluated numerically without difficulty. Both ψ_s and ψ_n ($n < K$) contribute to the steady state flow.

REFERENCES

Baines, P. G. 1977. Upstream influence and Long's model in stratified flow. *J. Fluid Mech. 82*, 147–159.

Baines, P. G. and Grimshaw, R. H. 1979. Stratified flow over finite obstacles with weak stratification. To appear *Geophys. Astrophys. Fluid Dyn.*

Clarke, T. L. and Peltier, W. R. 1977. On the evolution and stability of finite amplitude mountain waves. *J. Atmos. Sci. 34*, 1715–1730.

Davis, R. E. 1969. The two-dimensional flow of a stratified flow over an obstacle. *J. Fluid Mech. 36*, 127–143.

Gossard, E. and Hooke, W. 1975. *Waves in the atmosphere.* Elsevier. 456 pp.

Houghton, D. D. and Kasahara, A. 1968. Non-linear shallow fluid flow over an isolated ridge. *Comm. Pure & Appl. Math. 21*, 1–23.

Houghton, D. D. and Isaacson, E. 1970. Mountain winds. Studies in numerical analysis, 2: Numerical solutions of nonlinear problems, 21–52. Philadelphia: SIAM.

Klemp, J. B. and Lilly, D. K. 1978. Numerical simulation of hydrostatic mountain waves. *J. Atmos. Sci. 35*, 78–107.

Long, R. R. 1955. Some aspects of the flow of stratified fluids. III. Continuous density gradients. *Tellus 7*, 341–357.

Long, R. R. 1970. Blocking effects in flow over obstacles. *Tellus 22*, 471–480.

Long, R. R. 1974. Some experimental observations of upstream disturbances in a two-fluid system. *Tellus 26*, 313–317.

Lyra, G. 1943. Theorie der stationären Leewellenströmung in freier Atmosphäre. *Z. Angew. Math. Mech. 23*(1), 1–28.

McEwan, A. D. and Baines, P. G. 1974. Shear fronts and an experimental stratified shear flow. *J. Fluid Mech. 63*, 257–272.

McIntyre, M. E. 1972. On Long's hypothesis of no upstream influence in uniformly stratified or rotating flow. *J. Fluid Mech, 52*, 209–243.

Nicolls, J. M. 1973. The airflow over mountains. Research 1958–1972. World Met. Organ. Geneva. Tech. Note 127.

Queney, P. 1948. The problem of airflow over mountains: A summary of theoretical studies. *Bull. Am. Met. Soc. 29*, 16–26.

Queney, P., Corby, G. A., Gerbier, N., Koschmieder, H. and Zierep, J. 1960. The airflow over mountains. World Met. Org. Geneva. Tech. Note 34, 135 pp.

Smith, R. B. 1976. The generation of lee waves by the Blue Ridge. *J. Atmos. Sci. 33*, 507–519.

Su, C. H. 1976. Hydraulic jumps in an incompressible stratified fluid. *J. Fluid Mech. 73*, 33–47.

Trustrum, K. 1964. Rotating and stratified fluid flow. *J. Fluid Mech. 19*, 415–432.

Wei, S. N., Kao, T. W. and Pao, H.-P. 1975. Experimental study of upstream influence in the two-dimensional flow of a stratified fluid over an obstacle. *Geophys. Fluid Dyn. 6*, 315–336.

Wong, K. K. and Kao, T. W. 1970. Stratified flow over extended obstacles and its application to topographical effect on vertical wind shear. *J. Atmos. Sci. 27*, 884–889.

Yih, C. S. 1960. Exact solutions for steady two-dimensional flow of a stratified fluid. *J. Fluid. Mech. 9*, 161–174.

НАБЛЮДЕНИЯ СТРАТИФИЦИРОВАННОГО ТЕЧЕНИЯ НАД ДВУМЕРНЫМ ПРЕПЯДСТВИЕМ В ЖИДКОСТИ КОНЕЧНОЙ ГЛУБИНЫ

В статье описываются результаты экспериментального исследования стратифицированного течения над двумерным препятствием в жидкости конечной глубины при больших числах Рейнольдса и высотах препятствия около 1/10 глубины канала и меньше. Использовались длинные и короткие препятствия, и все детали поля течений описываются с некоторой степенью детальности. Наблюдения сравниваются с соответствующими теоретическими результатами, особенно с таковыми для линеаризованной модели потока над препятствием малой высоты. Для сверхкритических течений ($0 < K = ND/\pi U < 1$) линейная теория дает довольно аккуратное описание потока вплоть до значений, очень близких к критической скорости ($K = 1$), хотя решение линейной модели расходится при приближении к критической скорости. Для докритических потоков (где наблюдения были сконцентрированы в интервале $1 < K < 2$, содержащем лишь первую моду волн за препятствием) различные свойства поля волн достаточно хорошо описываются линейной теорией, однако другие аспекты потока описываются плохо, особенно, если поток лишь слегка докритичен. Несмотря на малость высоты препятствия существует конечный интервал параметров ($1 < K < K_c$), где устойчивая структура с модой 1 в виде столба существует в набегающем потоке ("влияние вверх по потоку") в том смысле, как это описано Бэйнсом (1977) для крупных препятствий, и этот тип движения не согласуется с теорией возмущений малой амплитуды. Эта особенность является, по всей видимости, постоянной при K_c, стремящемся к единице по мере приближения h к нулю. Поля скорости над препятствием выявляют соответствующие отличия от линейной теории и аналогичное поведение наблюдается для мод более высокого порядка. Эти явления должны иметь нелинейное происхождение и показывается, что они должны быть существенны для атмосферных потоков.